ESTIMATION OF HYDRAULIC FRACTURING POTENTIAL BY NUMERICAL ANALYSIS IN ROCKFILL DAM

Yukio Arai[1], Yoshiharu Kinouchi[2], Shiro Takeki[1], Atsunori Numata[1], Hiroto Fukushima[1] and Hideki Ohta[3]

INTRODUCTION It is considered that the hydraulic fracturing is a cause of rockfill dam failure. There is a possibility of hydraulic fracturing when vertical stresses in the core zone are not transmitted sufficiently because of nonuniformity, partial failure, erosion , etc., during and after the initial procedure of water storage. Therefore, evaluating a distribution of stress and strain in a dam is important to estimate the possibility of hydraulic fracturing for a certain part of the structure. Numerical analysis is needed to evaluate stress and strain in a dam. Kohgo (2000) carried out a deformation analysis for homogeneous earth dam during initial water storage using an elastoplastic model considering two effects of suction coupled with saturated-unsaturated consolidation analysis. Ng and Small (1999) presented a method of predicting hydraulic fracture in earth and rockfill dam based on the finite element method, and an example of analysis for the Hyttejuvet Dam. By that result, the failure of the dam was due to hydraulic fracturing during the initial water storage and the location where the hydraulic fracturing occurred in the simulation agreed with the location that the actual fracture was thought to be occurred.

In this paper, the hydraulic fracturing potential of the Surikami-kawa Dam in Japan during initial water storage was predicted using finite element analysis to estimate the stability of the dam. The model of the analysis is soil/water coupled consolidation analysis using the constitutive equation suggested by Sekiguchi and Ohta (1977). The parameters for this analysis are defined by the observation results and quality control tests during dam construction and the laboratory tests of dam materials. Resistance to hydraulic fracturing was defined by laboratory tests using a cylindrical specimen in standard triaxial cell. In addition, simulation cases with different incline angle of core zone and stiffness of filter zone were carried out to investigate the effect of these parameters.

ESTIMATION METHOD OF THE STABILITY AGAINST HYDRAULIC FRACTURING OF THE DAM

Condition for occurrence of hydraulic fracturing Though, in general, there is no collective opinion to define the hydraulic fracturing, a condition for occurrence of hydraulic

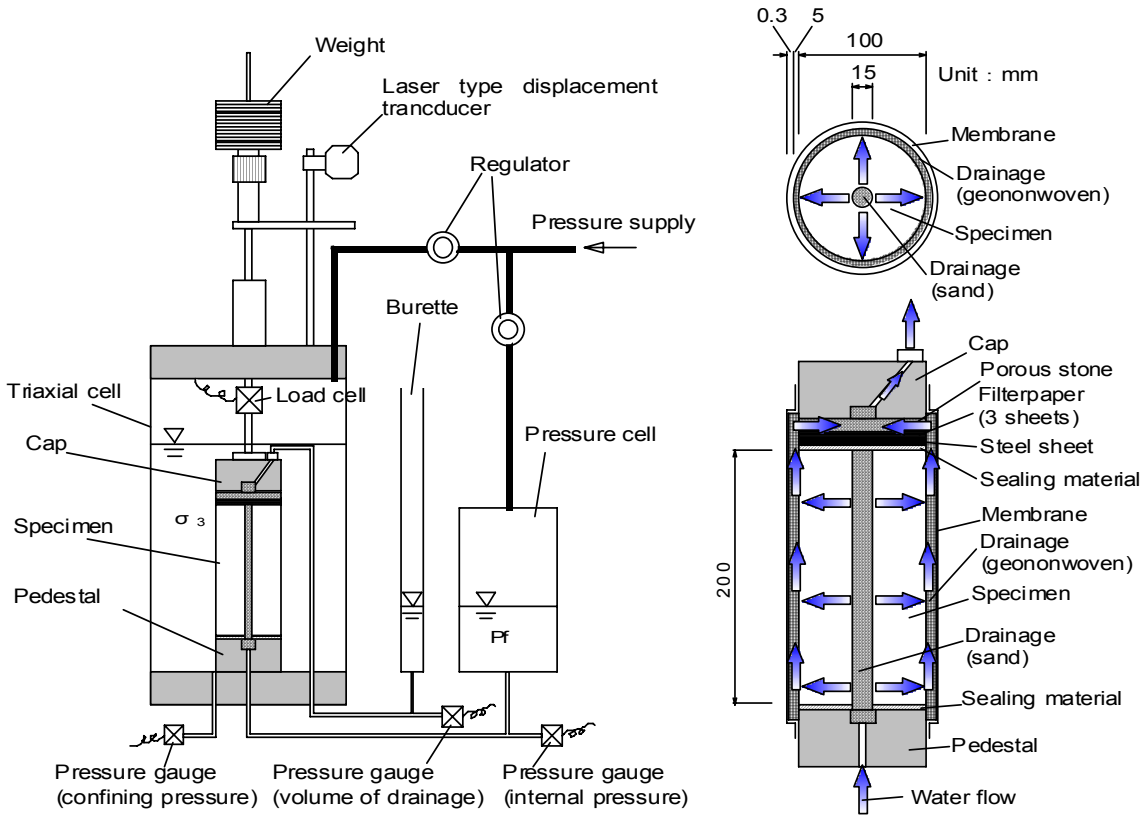

(a) The test apparatus (b) Water flow in the specimen

Fig. 1 Diagram of the test apparatus and the specimen

fracturing in this paper was defined as

$$u > m \times \sigma_3 + n \tag{1}$$

where u is the pore water pressure, σ_3 is the minor principal stress and m and n are coefficients obtained experimentally (Tagashira, 2002).

Laboratory experiment of hydraulic fracturing To apply Eq.(1) for hydraulic fracturing potential estimation using numerical analysis, a laboratory test using a cylindrical specimen in a standard triaxial cell was carried out. An actual rockfill dam material was used for the test. Although the maximum grain size was 150mm in the actual dam, the grain size distribution in the laboratory was adjusted to 9.5mm maximum grain size by excluding grains over 9.5mm. The soil was prepared at the corrected water content of 15.0% (maximum grain size 9.5mm) that corresponds to the actual grain size (maximum grain size 150mm). It was compacted to a prescribed density (dry density=1.87g/cm^3) that was corrected from the average density of the core zone using the Walker-Holtz method (Walker and Holtz, 1951).

Fig. 1 (a) shows a diagram of the test apparatus for hydraulic fracturing. The specimens were shaped into hollow cylinder that were 200mm in height, 15mm in internal diameter

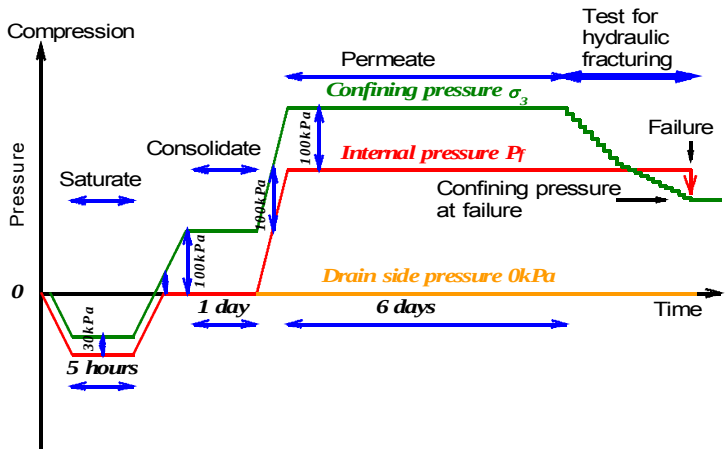

Fig. 2 Procedure of test for hydraulic fracturing

and 100mm in external diameter. The water flow in the specimen is shown in Fig. 1 (b). The reason for using hollow cylindrical shape was to achieve uniform radial water flow in the specimen.

Usually, in similar cases, increasing the internal pressure to failure is adopted. However, since the core material is impermeable, it takes long time to establish a steady state seepage. For this reason, the authors used the procedure shown in Fig. 2 to easily achieve a steady state seepage. It is also important to saturate specimens completely and finish the primary consolidation. The following steps were employed: first, to give a confining pressure for a specimens, internal pressure decreased up to -30kPa. Second, to saturate the specimens, both internal pressure and confining pressure decreased while keeping the same effective confining pressure. Third, deaired water was flowed into the specimens on the condition that the internal pressure was negative for about 5 hours. Fourth, the internal pressure was returned to atmospheric pressure, while keeping the same effective pressure. Fifth, to consolidate the specimens, the confining pressure increased up to 100kPa and was kept for about 1 day. Sixth, to produce a water flow, both internal pressure and confining pressure increased up to certain level, while keeping the effective confining pressure of 100kPa. Since the drain side pressure equals the atmospheric pressure, when the internal pressure increased, the flow in the specimens started. To attain the steady state seepage, as well as, to complete primary consolidation and saturation, the specimens were kept under this condition for about 6 days. Finally, to evaluate the hydraulic fracturing, confining pressure decreased step by step while keeping the same internal pressure. The internal and confining pressure were used as follows: (100kPa, 200kPa), (200kPa, 300kPa), and (300kPa, 400kPa).

Fig. 3 shows an example of time histories of confining pressure and volume of drainage. The change of drainage volume was initially very small but it increased rapidly at a certain stage while the confining pressure decreased gradually. This stage was defined as failure and the confining pressure at this point was measured.

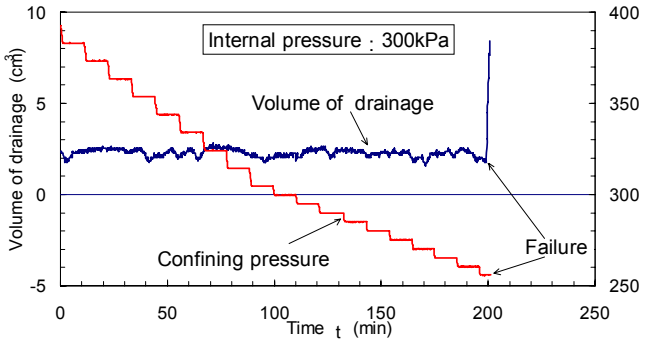

Fig. 3 An example of time histories of confining pressure and volume of drainage

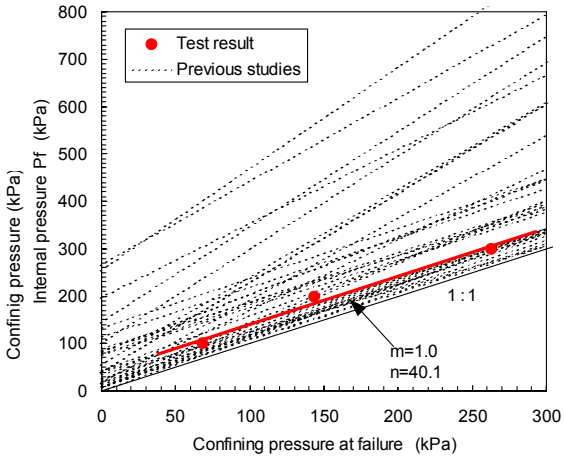

Fig. 4 Relationship between confining pressure at failure and internal pressure

In Fig. 4 the relationship between confining pressure at the failure and internal pressure is depicted. Test results were plotted linearly and it could be represented as Eq.(1) with m=1.0 and n=40.1. In addition, results of previous studies are also included in this figure. It can be seen that the lines of previous studies were distributed within a wide range and the specific test result was plotted almost at the lowest part of the range of distribution. To calculate the potential of hydraulic fracturing by means of safety factor, m=1.0 and n=0 were used in this study. The parameter n was set to zero in order to examine the worst case.

OUTLINE OF THE SURIKAMI-KAWA DAM AND MODEL OF ANALYSIS

Outline of the Surikami-kawa dam The Surikami-kawa dam is a central core type rockfill dam with height of 105m, crest length of 718.6m and volume of 8,300,000m^3. Fig. 5 shows the cross section of the Surikami-kawa dam. This cross section, namely No.28, was selected because it is the maximum and many gauges and measurement points are set. The arrangement of the earth pressure gauges, pore water pressure gauges and differential settlement gauges is seen in Fig. 6.

Outline of numerical analysis Mori et al. (2003) reported the behavior of a fill dam by

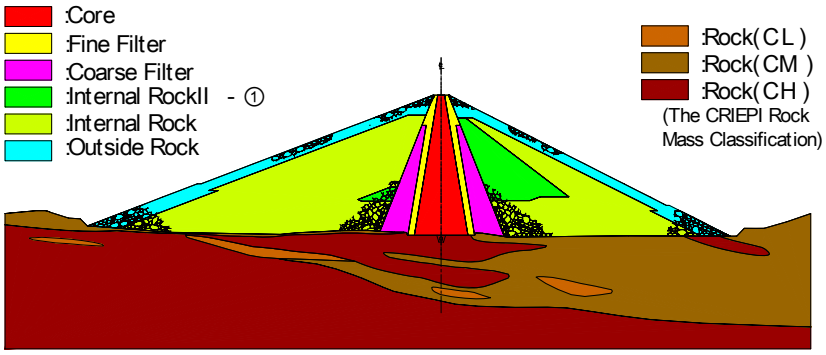

Fig. 5 Cross section of the Surikami-kawa dam

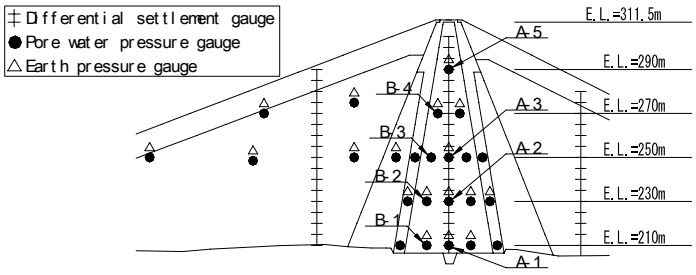

Fig. 6 Arrangement of gauges and measuring points

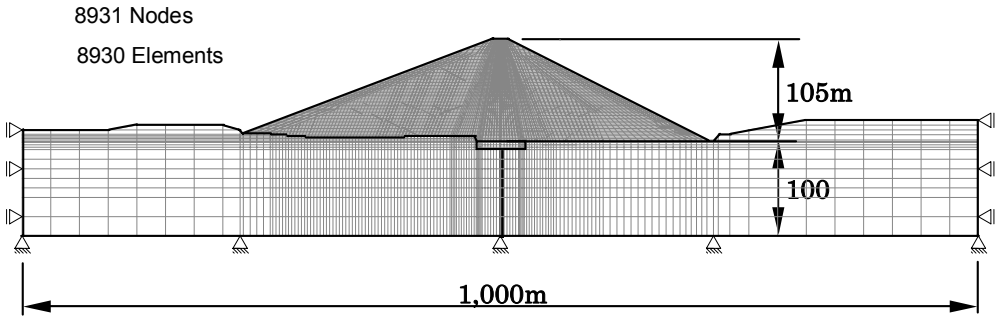

Fig. 7 Finite element model of the Surikami-kawa dam

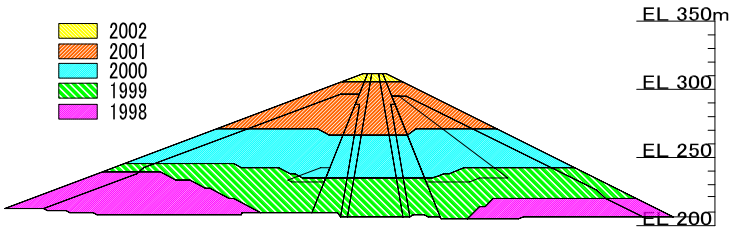

Fig. 8 Areas of filling of the dam each year

soil/water coupling analysis of Sekiguchi and Ohta model, which assumes all filling materials of the dam as elasto-viscoplastic. They also estimated the potential of the hydraulic fracturing for a large rockfill dam. They considered dam materials as over-consolidated soil while the effect of compaction meant a pre-compressive stress. The 2 dimensional effective stress analysis code used in this paper is DACSAR (Iizuka and Ohta, 1987). The finite element mesh is shown in Fig. 7.

To reproduce the accurate performance of the rockfill dam, the shape and the process of construction were modeled accurately from the construction process to the water storage process continuously. The construction lasted five years. The areas of dam filling for each year are depicted in Fig. 8. The time history of the filling of the core zone is shown in Fig. 9. Since the Surikami-kawa dam is located at a site where it has snow in winter, there was a pause of construction every year. It is important to model even this process. Although for the initial procedure of water storage, three cases were assumed, (average year, water shortage year and rainy year), the actual recent process of water storage was adopted for the simulation. Fig. 10 shows the procedure of water storage. It took about one year to reach the surcharge water level.

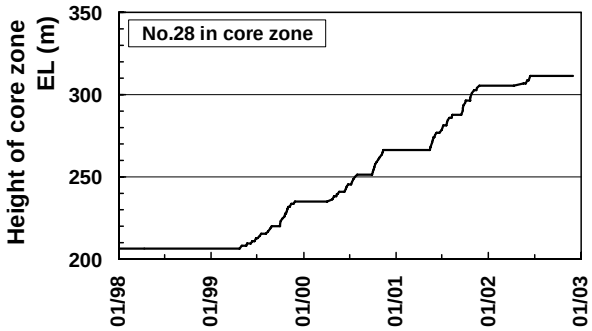

Fig. 9 Time history of filling of the dam

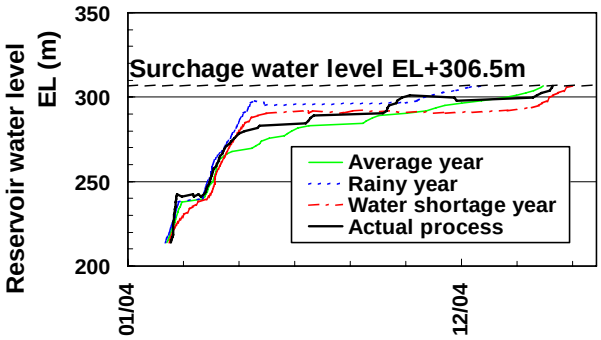

Fig. 10 Time history of water storage

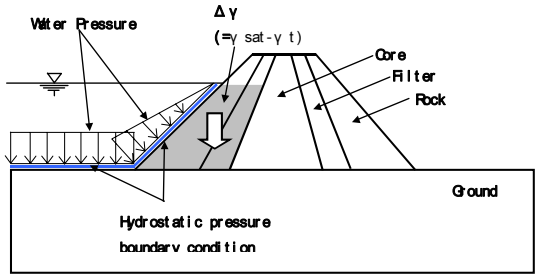

Fig. 11 Modeling of water storage

Conditions of analysis The displacement and the water boundary conditions used in the soil/water coupling analysis were set similar to Mori et al. (2003). Additionally, the load of the reservoir water was set the same as in Mori et al. (2004). Side boundaries were fixed to horizontal direction for displacement and drained hydrostatic pressure for water condition. Bottom boundaries were fixed and drained hydrostatic pressure for water condition was applied. For the rock and filter zone the following condition applied. In order to fix the pore water pressure to zero, the boundary condition that the pore water pressure equals zero was used at the upper and lower plane of each element. Additionally, the drain boundary condition was set at the upper and lower plane of each element. For the surface of the core zone, drain boundary conditions were applied and the condition that the pore water pressure equals zero. When a new element was added above the previous layer, these pore water pressure and drain boundary conditions were removed and the previous surface of the element became internal plane. In addition, the drain condition was set at a boundary between the core and the filter zone.

Fig. 11 shows the modeling of water storage (Mori et al., 2004). The load of water storage was assumed to act as hydrostatic pressure on the surface of the upstream rock and the ground. The hydrostatic pressure boundary condition corresponding to the water storage level was set on the surface of the upstream rock, and the water boundary conditions were removed in the rock and the filter zone in the upstream side simultaneously, when the water level rose to each node or higher. The unit weight of the rock and filter materials in the upstream zone increased from moist weight (γ_t) to saturation weight (γ_{sat}). Therefore, the vertical load due to the difference of these unit weights ($\Delta\gamma=\gamma_{sat}-\gamma_t$) acted on each element.

Parameters The values of physical properties were determined from the quality control

tests, laboratory tests and observation data during dam construction. Some parameters, however, especially for the filter, could not be obtained from laboratory test or observation, because there was no specific filter material for the laboratory test and no measuring point of the differential settlement in the filter zone. For this reason, the parameters concerning the filter were assumed to be consistent with observation data in the rock and the core zone. Additionally, since the coefficient of permeability for the core zone, that was obtained from the laboratory test, was considerably smaller than that obtained from the quality control test, the latter was used, because it was in agreement with generally accepted values. Parameters of the numerical analysis are shown in Table 1.

RESULT OF NUMERICAL ANALYSIS AND ESTIMATION OF HYDRAULIC FRACTURING POTENTIAL

Pore water pressure, displacement and stress during dam construction Fig. 12 shows the variation of pore water pressure, vertical displacement and stress at some measurement points (A-1 and A-3) of EL210m and 250m in the core zone as shown in Fig. 6 during dam construction. The pore water pressure increased during the filling of the core zone and dispersed during the pauses of construction, while it dispersed earlier than that of the measurement values. This is considered to be due to the difference of the coefficient of permeability obtained by the quality control test and the actual one.

The settlement (vertical displacement) at EL250m in the core zone rapidly increased during dam construction, see Fig. 12 (b). It decreased slowly during the pause of construction with

Table 1 Parameters used for the analysis

Material Properties \ Zone		Core	Fine Filter	Coarse Filter	Rock II	Rock II -1	Rock I	Base Rock	Grouting
Wet density ct (t/m^3)		2.25	2.29	2.20	2.13	2.11	2.11	2.20	2.20
Satureted density csat (t/m^3)		_	2.31	2.28	2.26	2.22	2.21	-	-
Void ratio corresponding to y_{v0}' e_0		0.37	0.15	0.19	0.23	0.23	0.28	-	-
Pre-consolidation stress pc(kPa)		200	470	500	280	200	500	-	-
Compression index л		0.013	0.0087	0.0087	0.024	0.026	0.0846	-	-
Swelling index к		0.0035	0.0022	0.0022	0.0028	0.0022	0.0021	-	-
Internal friction angle ц' (°)		47.4	50.8	51.6	51.7	50.4	50	-	-
Young's modulus E(kPa)		-	-	-	-	-	-	2.8E+06	2.8E+06
Coefficient of permeability k	(m/day)	1.0E-03	2.3E+00	1.8E+01	5.6E+01	4.6E+01	9.2E+01	1.0E-02	2.4E-06
	(cm/s)	1.2E-06	2.6E-03	2.0E-02	6.5E-02	5.4E-02	1.1E-01	1.2E-05	2.7E-09
Plasticity index IP		21.4	-	-	-	-	-	-	-
Coefficient of dilatancy D		0.0036	0.0027	0.0026	0.0081	0.0093	0.0312	-	-
Irreversibility ratio Л		0.73	0.75	0.75	0.88	0.92	0.98	-	-
Critical State parameter M		1.95	2.09	2.12	2.13	2.08	2.06	-	-
Effective Poisson's ratio н'		0.35	0.31	0.31	0.31	0.31	0.31	0.3	0.3
Coefficient of earth pressure at rest K_0		0.53	0.45	0.45	0.45	0.45	0.45	-	-
Thickness of banking element (m)		1.5	1.5	1.5	1.5	1.5	1.5	-	-
Effective overburden pressure y_{vi}' (kPa)		9.3	9.7	9.0	8.5	8.3	8.3	-	-
Overconsolidation ratio OCR		21.4	48.4	55.5	33.0	24.0	60.1	-	-
Coefficient of in-site earth pressure Ki		2.12	3.54	3.81	2.88	2.43	3.96	-	-
Coefficient of secondary compression б		4.8E-04	3.8E-04	3.7E-04	9.8E-04	1.1E-03	3.3E-03	-	-
Gradient of coefficient of permeability $л_k$		0.010	0.0087	0.0087	0.024	0.026	0.0846	-	-

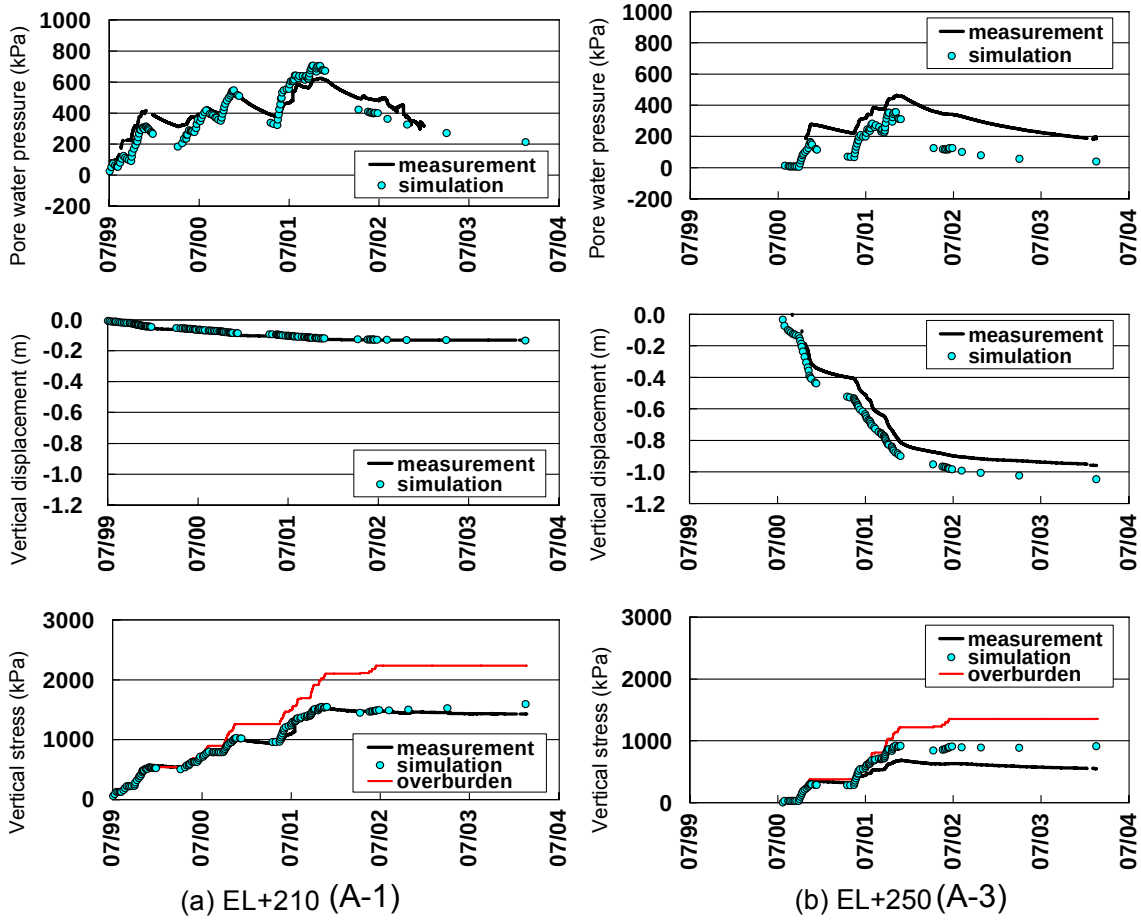

Fig. 12 Variation of pore water pressure, vertical displacement and earth pressure during dam construction

the dispersion of pore water pressure. The settlement of A-1 is not considered important, as see in Fig. 12 (a). In addition, it seems that the settlement can be estimated using this model not only qualitatively but also accurately. Total vertical stresses are also compared in Fig. 12. It can be calculated that the total vertical stress of measurement and simulation are 40 to 80 % of the overburden pressure as shown in the bottom of Fig. 12.

Fig. 13 shows the contour of effective vertical stress at the end of the filling of the dam. It can be seen that the effective vertical stress concentrates in the filter zone; on the other hand, in the core zone it is obviously smaller because of the stiffness difference of the filter and

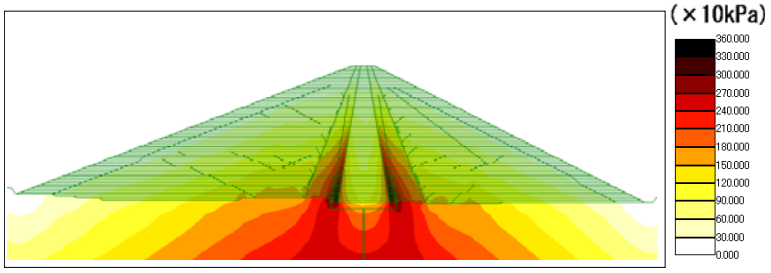

Fig. 13 Contour of effective vertical stress at the end of dam construction

the core zone. This is why the total vertical stress from measurement and simulation in the core zone is smaller than that of the overburden pressure.

Pore water pressure and stress during the water storage Fig. 14(a)depicts the simulation and measurement results of pore water pressure at the measurement points in the upstream core zone during dam construction and water storage. In the early stage of water storage, the simulation results of pore water pressure were generally lower than the measurement data. However, in the final stage of water storage, the difference between measurement and simulation decreased. Fig. 14(b) depicts the total vertical stress at the measurement points in

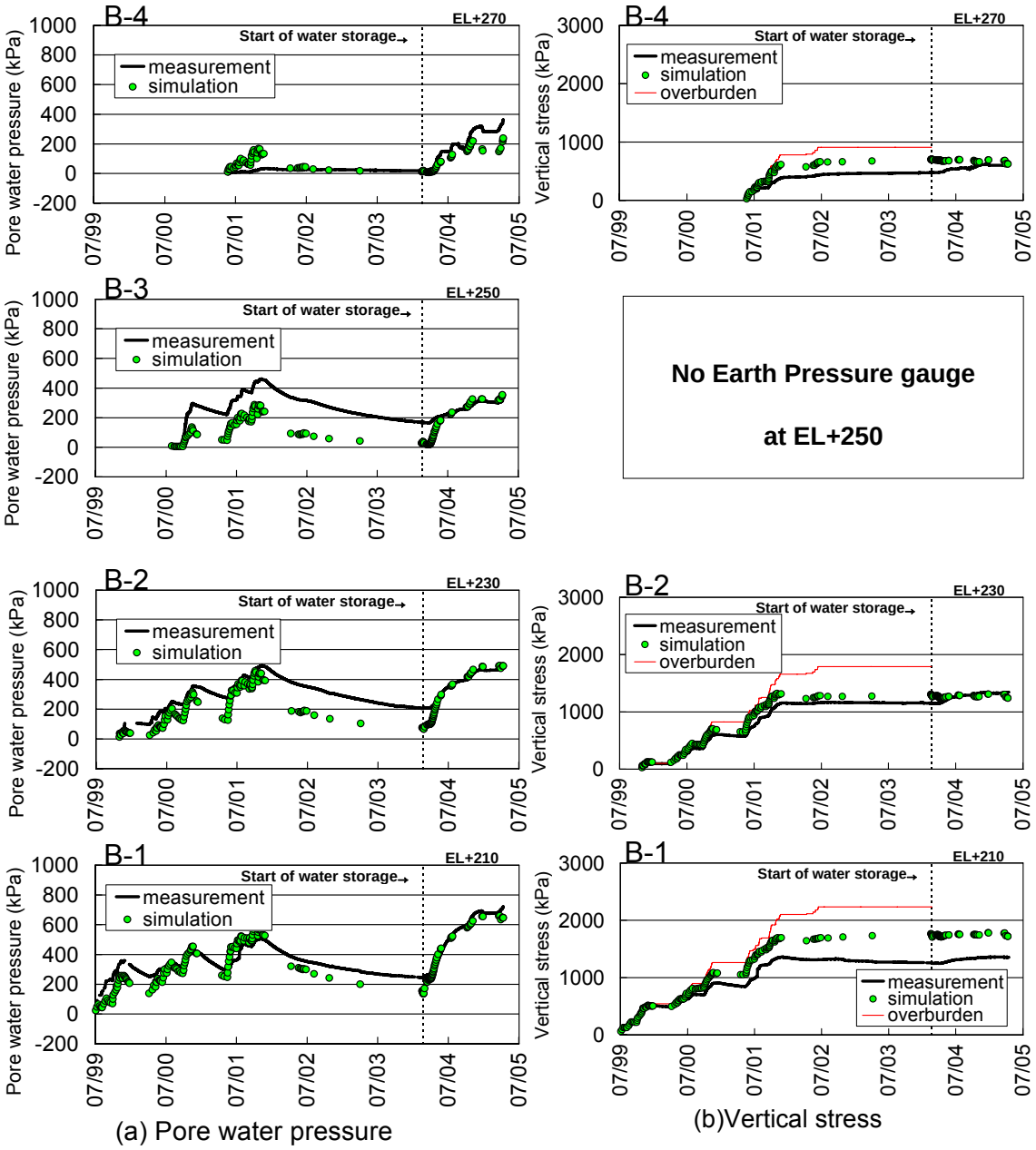

Fig. 14 Analysis and measurement results at the measurement points in the upstream core during water storage

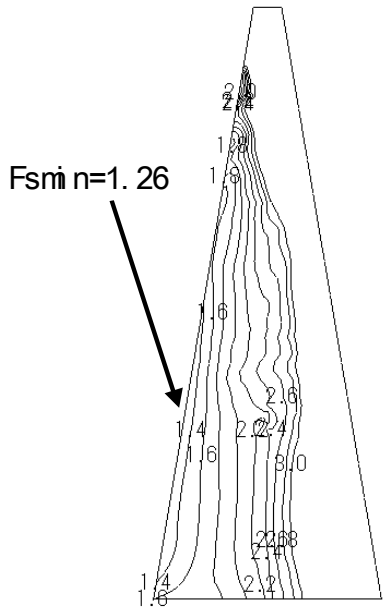

Fig. 15 Contour of safety factor against HF in the core zone

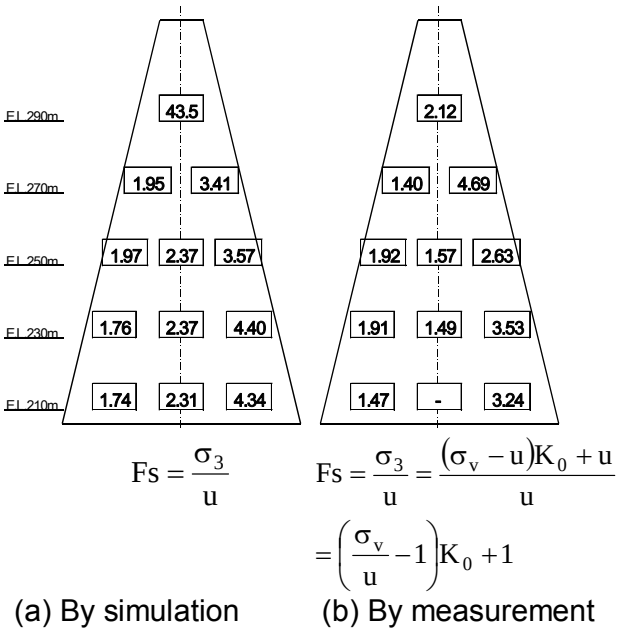

σ_1: Major principal stress
σ_3: Minor principal stress
u: Pore water pressure
σ_v: Vertical pressure
K_0: Coefficient of earth pressure at rest

Fig. 16 Safety factor at the measuring points

the upstream core zone during dam construction and water storage. It can be seen that the simulation results are similar to the measurements, although somewhat higher.

Estimation of hydraulic fracturing (HF) potential Using the Eq.(1), the safety factor against the HF as a HF potential can be presented as follows:

$$F_s = \frac{m\sigma_3 + n}{u} \tag{2}$$

Since m=1.0 and n=0 as described above, Eq.(2) can be converted as follows:

$$F_s = \frac{\sigma_3}{u} \tag{3}$$

Fig. 15 shows the contour of safety factor against HF in the core zone at the time the water storage level reached the surcharge water level. σ_3 and u were results of simulation. The minimum safety factor against HF is more than 1.2 at the surface of the upstream and at a height somewhat under the center of core zone. The safety against HF could, therefore, be confirmed for the Surikami-kawa dam.

The safety factors obtained by simulation and measurement are shown in Fig. 16 (a) and (b) respectively. The differences between simulation and measurement are considerably small except the values at the highest position. In the simulation, every element was assumed under the saturated condition, but the actual condition near the top surface area was

considered unsaturated. This is why there was a great difference between the simulation and the measurement near the top surface area in the core zone.

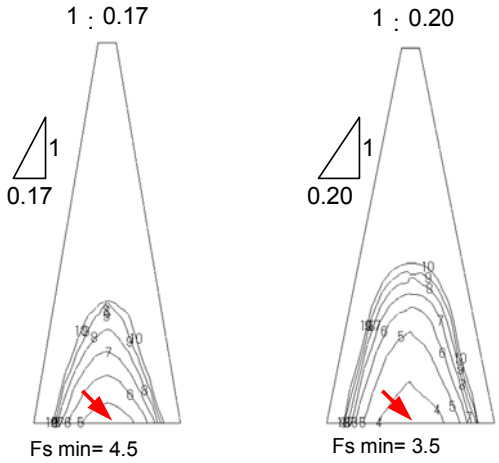

Fig. 17 Contour of safety factor against HF of Case 1

EXAMPLES OF DIFFERENT SHAPE AND STIFFNESS OF THE DAM The Surikami-kawa dam is a rock-fill dam of the central core type with the incline angle of the core zone of 1:0.17. This incline angle is considered steep, whereas usually it is 1:0.2. In this paper, the two following cases were examined:

Case 1) The incline angle of the core zone is changed to 1:0.2 with the same width of the core at the top,

Case 2) The stiffness of the filter is changed.

The numerical analysis for these simulations used a simplified model with 3,000 elements and 3,000 nodes. The analysis was carried out until the end of the filling of the dam, and not until the end of water storage, because the qualitative relationships of safety factor are considered similar. The comparison of the contours of the safety factors against HF between 1:0.17 and 1:0.20 are shown in Fig. 17. The safety factor of incline angle of 1:0.17 is higher than that of 1:0.2. It is considered that the dispersion of pore water pressure in the core zone is faster for the 1:0.17 than the 1:0.20, because the drain length of the core zone in the first case is smaller.

Fig. 18 shows the contour of safety factor against HF for Case 2. The safety factor against

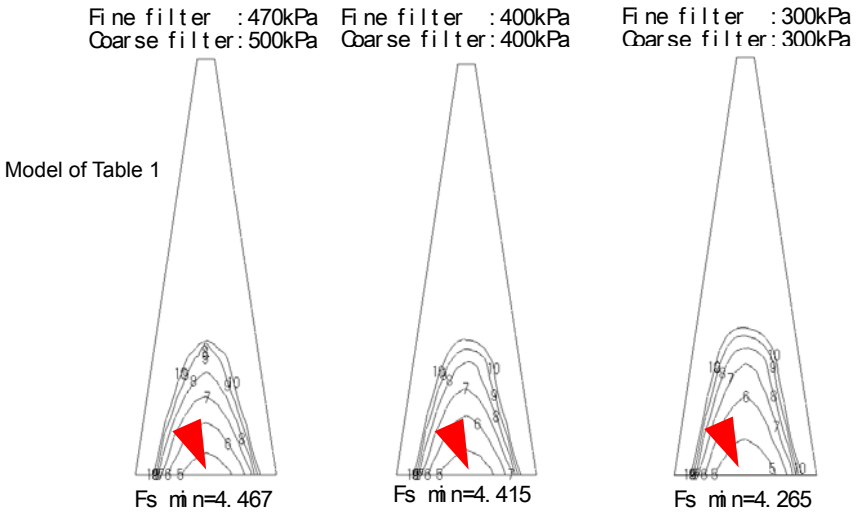

Fig. 18 Contour of safety factor against HF of Case 2

HF slightly decreased with decreasing stiffness of the filter zone, although it was expected to increase with decreasing filter stiffness, as suggested from Fig. 13. However, it can be seen that the safety factor of HF is not dominated by the difference of stiffness of the filter zone.

CONCLUSION The model presented in this paper can estimate the performance of a dam during and after construction by setting parameters obtained from laboratory tests, quality control tests and measurement data. For some parameters estimated values had to be applied because some materials could not be obtained and there was no settlement measuring point. Using this model, the safety of this dam against hydraulic fracturing could be confirmed and an example of hydraulic fracturing estimation is discussed in this paper. Certain issues to be dealt with in the future would be a laboratory test method to determine the material properties and a way to correlate them to the actual condition of the rockfill dam.

REFERENCES

1) Iizuka, A. and Ohta, H. A Determination Procedure of Input Parameters in Elasto-visco Plastic Finite Element Analysis, *Soils and Foundations*, Vol.27, No.3, Japan(1978)71-87

2) Kohgo, Y. Behavior of fill-type dam during reservoir filling and its analysis method, *Large Dams*, No.171, Japan(2000)15-27 (in Japanese)

3) Mori, Y., Uchita, Y., Shimokawa, Y., Yoshikoshi, H. ,Ishiguro, T., and Ohta, H. Stress and deformation analysis of a center core-type rockfill dam during construction, *Proceedings of the Japan Society of Civil Engineers*, No.743, Ⅲ-64, Japan(2003)105-124 (in Japanese)

4) Mori, Y., Uchita, Y., Tsuruta, S., Takahashi, A., Ishiguro, T., and Ohta, H. Estimation of Hydraulic Stability of a center core-type rockfill dam, *Proceedings of the Japan Society of Civil Engineers*, No.764 Ⅲ-67, Japan(2004)69-84 (in Japanese)

5) Ng, A. K. L. and Small, J. C. A case study of hydraulic fracturing using finite element methods, *Can. Geotech. J.*, Vol.36, Canada(1999)861-875

6) Sekiguchi, H. and Ohta, H. Induced anisotropy and time dependency in clay, *9th ICSMFE, Tokyo*, Proc. Speciality session 9, Japan(1977)229-239

7) Tagashira, H. On the proportional coefficient and constant of linear approximate equation between hydraulic fracturing pressure and minimum confining pressure based on literature review, *Symposium on seepage failure of ground and its evaluation*, The Japanese Geotechnical Society, Japan(2002)141-148 (in Japanese)

8) Walker, F. C. and Holtz, W. G. Control of embankment material by laboratory testing, *Proc. ASCE*, No.108, USA(1951)1-25

[1]Tobishima Corporation

[2]Ministry of Land, Infrastructure and Transport Japan

[3]Tokyo Institute of Technology